# Numerical Analysis of a Natural and Excited Two-Dimensional Mixing Layer

A. Kourta,* M. Braza,† P. Chassaing,‡ and H. Haminh§
*Institut de Mecanique des Fluides de Toulouse, Toulouse, France*

**Physical properties of a two-dimensional plane mixing layer are examined by numerical solution of the unsteady Navier-Stokes equations using a pressure velocity formulation. The natural (unforced) mixing layer due to the merging of two streams with a velocity ratio ($r=0.33$) is studied at Reynolds numbers $Re=200$, 500, and 1000. Different transition zones are detected: stable, linear, and nonlinear. The roll-up process appears in the nonlinear zone. The main flow features are in agreement with the experimental evidence. The excited mixing layer at the first subharmonic and at the incommensurate frequency are investigated to analyze the coalescence mechanism and the nonlinear interaction.**

## I. Introduction

THE merging of two streams initially separated by a thin surface plays an important role in numerous applications such as aerodynamics and combustors. Experiments reported by a number of authors have shown that orderly structures are extant in the turbulent mixing layer. Visualization studies reported by Brown and Roshko[1] confirm that large-scale coherent structures are indeed intrinsic features of the turbulent mixing layer at high Reynolds numbers. Furthermore, sequential mergings of the vortices constitute the primary mechanism for the spreading of the mixing layer in the downstream direction, as pointed out by the experiments of Winant and Browand.[2] These observations have had a major impact on the understanding of turbulence in free shear flows.

The large-scale vortices are observed not only in the early laminar stages of the flow, but also farther downstream in the turbulent region, where they coexist with a fine-scale motion. Hence, two issues need to be examined: the evolution of the large eddies identified in the viscous laminar flow and the link between these eddies and the coherent structures observed in the turbulent flow.

The mechanisms of transition and coherent structures play an important role in the correct modeling of turbulent flows. Two main approaches are currently used in the experimental and theoretical analyses used to study these mechanisms: the classical linear hydrodynamic stability theory and the description of vorticity field in the physical space.

In the classical hydrodynamic stability theory, the mixing layer is viewed as an overlapping of the instability waves that propagate and amplify in the downstream direction. The flow is naturally described in the Fourier space. Therefore, measured data in the frequency space cannot be easily related to the evolution of the orderly structures.[3,4]

The second approach, by taking into account the nonlinear character, explains the behavior of coherent structures by studying the evolution of the vorticity field in the physical space. The structures are considered to be vortices of a characteristic size that exhibit different types of interactions.[5,6] In this case, the results can be compared with the flow visualization studies.

The initial development of the mixing layer is described very satisfactorily by the linear stability theory. This state is followed by the establishment of fully rolled-up vortices shed at the frequency $f_n$. This is a strongly nonlinear process. Experimental observations indicate that the roll-up process is predominantly two-dimensional. When the fundamental component of mixing layer frequency $f_n$ reaches its maximum amplitude, it is followed by the generation of a subharmonic component at $f_n/2$. The emergence of this component at half the frequency of the fundamental constitutes one of the most striking features in the mixing layer dynamics, as detected by Freymuth.[7] The selective growth of the subharmonic component leads further downstream to the pairing of neighboring vortices, as observed in the flow visualization studies made by Winant and Browand.[2] This phenomenon occurs randomly along the downstream direction and is followed by an approximately two times increase in the momentum thickness.

Quantitatively, parameters that influence the dynamics of free shear layer flows are, particularly, the velocity ratio, Reynolds number, and initial state of the boundary layer (turbulent or laminar).

A mixing layer is characterized by two distinct velocity scales: the velocity difference $dU$ that quantifies the spreading rate of the orderly structures and the average velocity $\bar{U}$ that is approximately the convection velocity. The velocity ratio $r=dU/2\cdot{}^{*}\bar{U}$ compares these two velocity scales. It is found that the maximum growth rate is approximately proportional to the velocity ratio.[8] Likewise, the dynamics of the mixing layer depend on the Reynolds number. It is also known that the downstream development of the shear layer is very sensitive to the laminar or turbulent state of the initial boundary layer. The spreading rate of turbulent mixing layers ($r\neq 1$) is usually found to be much lower than the corresponding laminar value.[9] The sensitivity of the shear layer to initial conditions is most readily illustrated by the effect of a varying excitation frequency $f_f$.[10] Ho and Huerre[11] pointed out that, within the range $\frac{1}{2}f_n<f_f<2f_n$, the response frequency $f_r$ is found to be equal to $f_f$; hence, vortices are shed at the forcing frequency. When $\frac{1}{4}f_n<f_f<\frac{1}{2}f_n$, the response frequency $f_r$ jumps to the first harmonic $2\times f_f$ closer to the natural frequency $f_n$. Neighboring vortices are then laterally displaced and subsequently wrap around each other to form a single structure.

The present paper is a numerical study of the dynamics of a two-dimensional mixing-layer flow of homogeneous, incompressible viscous fluid at moderate Reynolds numbers.

Actually, the numerical results analysing the nonlinear mechanisms among different modes in such a flow are rather

Received Oct. 30, 1985; revision received June 16, 1986.


*Research Scientist.
†Chargé de Recheche au CNRS.
‡Maître de Conference.
§Professor. Member AIAA .

scarce. For this reason, the complete nonlinear Navier-Stokes and continuity equations are solved by a pressure velocity formulation. The theoretical and numerical approach are presented in Sec. II. The results concern first the nonperturbed mixing layer (Sec. III.A). The spreading rate of the mixing layer and the interaction of pressure and velocity fields are studied. The natural frequency of the eddies motion is evaluated. Finally, the forced mixing layer case is examined (Sec. III.B). The pairing mechanism and nonlinear interactions among different frequencies are discussed.

## II. Theoretical and Numerical Approach

### A. Governing Equations and Numerical Method

The equations are those of isothermal and incompressible viscous flow. They are written in conservative form as follows:

$$\frac{\partial(U_i)}{\partial X_i}=0 \tag{1}$$

$$\frac{\partial(U_i)}{\partial T}+\frac{\partial(U_iU_j)}{\partial X_j}=-\left(\frac{1}{\rho}\right)\frac{\partial(P)}{\partial X_i}+\frac{\nu\cdot\partial^2(U_i)}{\partial X_j\cdot\partial X_j} \tag{2}$$

These equations can be written in dimensionless form as

$$\frac{\partial(\tilde{U}_i)}{\partial\tilde{X}_i}=0 \tag{3}$$

$$\frac{\partial(\tilde{U}_i)}{\partial\tilde{T}}+\frac{\partial(\tilde{U}_i\tilde{U}_j)}{\partial\tilde{X}_j}=-\frac{\partial(\tilde{P})}{\partial\tilde{X}_i}+\left(\frac{1}{Re}\right)\frac{\partial^2(\tilde{U}_i)}{\partial\tilde{X}_j\cdot\partial\tilde{X}_j}\qquad i=1,2 \tag{4}$$

with the following dimensionless variables: $\tilde{X}=X/L_{\text{ref}}$, $\tilde{U}=U/U_{\text{ref}}$, $\tilde{T}=T/T_{\text{ref}}$, $T_{\text{ref}}=L_{\text{ref}}/U_{\text{ref}}$. The Reynolds number is defined as $Re=L_{\text{ref}}*U_{\text{ref}}/\nu$, where $L_{\text{ref}}=b_0$, the initial boundary thickness, and $U_{\text{ref}}=U_1$.

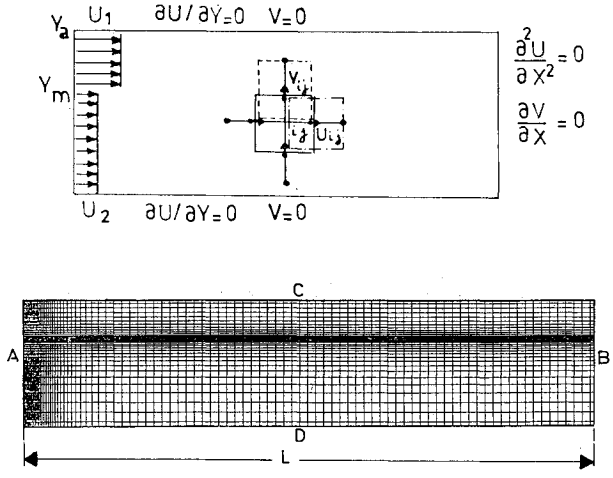


**Fig. 1 Geometrical domain and boundary conditions.**

The numerical method used to solve the previous equations is developed by Braza.[12] It is a pressure-velocity, finite-volume, semi-implicit, second-order accurate numerical method based on a predictor-corrector pressure scheme proposed by Chorin.[13]

The method consists of solving the momentum equations at time step $(n+1)Dt$ for an approximate velocity field $V^*$, by using a guess pressure $P^*=P^n$. The $V^*$ field is related to $V^{n+1}$ by an auxiliary potential function $\phi$, which is calculated by a Poisson equation, claiming that $\text{div}(V^{n+1})=0$. The pressure is then calculated by $P^{n+1}=P^n+\phi/Dt$. This procedure is repeated at each time step.

The momentum equations are solved by an alternating direction implicit (ADI) method developed by Peaceman and Rachford.[14] The Poisson equation for $\phi$ is solved by an ADI iterative method.

The time and space accuracy were shown to be of second order by applying the present method in the Taylor problem,[15] for which the analytic solution is available as a function of $x$, $y$, $t$, and Reynolds number.

A more detailed description of the method used and of its accuracy are given in Refs. 12, 16, and 17.

### B. Boundary Conditions and Computation Domain

The calculation domain is rectangular, as shown in Fig. 1. Its size is chosen to simulate the flow correctly and to minimize the influence of boundary conditions. The number of nodes is $102\times36=3672$. The size of the calculation domain is 67.67 in the horizontal direction and 14.69 in the lateral one, in terms of dimensionless variables.

*Numerical Parameters*

Two different mesh sizes are used. The first was an equidistant mesh with $DX=DY=0.1$. Nevertheless, the external boundaries were too close to the vortex region. The second is a variable mesh spacing in each direction (Fig. 1): in the $x$ direction, an equidistant mesh space is adopted for the first 20 nodes ($DX=0.1$). Then, the spacing grows exponentially to obtain a large domain, while preserving the accuracy. The spacing does not stretch more than 20% from cell to cell.

In the $y$ direction, an equidistant mesh space is adopted for the intermediate zone ($18<J<24$) with $DY=0.1$, where the main phenomena take place. On both sides of this region, an exponential growth of the mesh sizes is used (with $DY_{\max}=0.9$). The other numerical parameters are given in Table 1.

A detailed study of the grid independency of the solution and the space and time resolution required for the Reynolds numbers chosen can be found in Refs. 12 and 17 for other nonconfined flows. Hence, the mesh spacing, time step, and dimensions of the flow domain, adopted for the present case, are based to the above-mentioned studies in order to provide a physically valid solution.

**Table 1 Numerical parameters[a]**

| $Re$ | $DT$ | $N_x$ | $N_y$ | $N$ | $M$ | $T^*$ | CPU/$Dt$ | Total, CPU, s |
|---|---|---|---|---|---|---|---|---|
| 200 | 0.01 | 102 | 36 | 14688 | 470K | 80 | 1.8 | 240 |
| 500 | 0.01 | 102 | 36 | 14688 | 470K | 80 | 1.9 | 253.33 |
| 1000 | 0.01 | 102 | 36 | 14688 | 470K | 80 | 2.0 | 266.66 |

[a] $N_x$ is the number of nodes in $x$ direction, $N_y$ the number of nodes in $y$ direction, $N$ the number of unknowns, $M$ the memory storage required, $T^*$ the dimensionless physical time.

*Boundary Conditions*

At section A in Fig. 1, the inlet boundary conditions are

$$U(X_m, Y) = 1 \quad \text{for} \quad Y_m < Y < Y_a \tag{5a}$$

$$U(X_m, Y) = 0.5 \quad \text{for} \quad 0 < Y < Y_m \tag{5b}$$

$$V(X_m, Y) = 0 \quad \text{for} \quad 0 < Y < Y_a \tag{5c}$$

The physical domain of the flow is not confined. Nevertheless, fictitious boundaries are needed in order to solve the Navier-Stokes equations numerically. The choice of the boundary conditions is an important problem in order to confine as little as possible the calculation domain of the present exterior flow.

Hence, at outlet section B (Fig. 1), the free boundary-layer type of condition are taken to be

$$\frac{\partial^2 U}{\partial X^2} = 0 \tag{6a}$$

$$\frac{\partial V}{\partial X} = 0 \tag{6b}$$

These conditions are less restrictive and more physical than

$$\frac{\partial U}{\partial X} = 0 \quad \text{and} \quad V = 0 \tag{7}$$

which assume that the flow becomes parallel beyond a long distance. Actually, the use of Eqs. (7) need a very long distance $L$ to reach the parallel flow. Equations (6) need a shorter length $L$. They state that neither the $V$ component nor first derivative of the $U$ component change in the $x$ direction. In fact, these two conditions correspond to the physical development of the present wake flow far from the initial velocity gradient. Moreover, it is verified that these conditions allow the eddies to be freely developed downstream as they leave the flow domain. See Fig. 2.

The boundaries C and D are also fictitious and used for a numerical goal. The boundary conditions along these lines must allow the entrainment of the outer region in the flow domain. They must also simulate a quasiparallel flow at infinity. Three kinds of boundary conditions are tested:

1) The first is a Neumann condition,

$$\frac{\partial U}{\partial Y} = 0 \quad \text{(symmetry condition)} \tag{8a}$$

$$\frac{\partial V}{\partial Y} = 0 \tag{8b}$$

In order to satisfy the continuity equation (8b) implies that $\partial U/\partial X = 0$ along the sections C and D. Therefore, these boundary condtions are based on the hypothesis that the flow has an irrotational behavior at infinity.

2) The second boundary condition is similar to the first from a physical point of view, but numerically it is more restrictive, as

$$U = Cte \quad \text{and} \quad \frac{\partial V}{\partial Y} = 0 \tag{9}$$

3) Finally, the impermeability and symmetry conditions are tested,

$$V = 0 \quad \text{and} \quad \frac{\partial U}{\partial Y} = 0 \tag{10}$$

They are based on the hypothesis that these boundaries are streamlines.

Note that, with these boundary conditions, the Navier-Stokes equation for $V$ component is written as

$$P = \mu \cdot \left( \frac{\partial V}{\partial Y} \right) \tag{11}$$

This linear equation shows that $V$ is directly related to $P$ along these sections. The initial conditions are taken those of the inlet section.

The choice between the three types of boundary conditions along the sections C and D is made by numerical tests using the same grid and initial conditions.

Conditions 1 and 2 gave acceptable results only for dimensionless time $T < 10$. After that, the velocity field indicates that the growth of the mixing layer is perturbed by the boundary conditions. See Fig. 3. It is also observed that after $T = 50$ the values of div($V$) rise dramatically. Thus, the mass conservation is no longer verified. Hence, those conditions associated with the present size of the calculation domain are not compatible with the expansion of the mixing layer.

Boundary condition 3 leads to a more successful calculation. In fact, the values of div($V$) are found to be less than $10^{-5}$ in the whole field. Moreover, the mixing layer is found to grow in accordance with a physical process. These boundary conditions are then compatible with the size of the domain and do not confine the flow in the present case (Fig. 2).

## III. Results

The results concern two types of mixing layers according to the inlet velocity profile (Fig. 4). The first corresponds to the merging of two initially uniform parallel streams termed

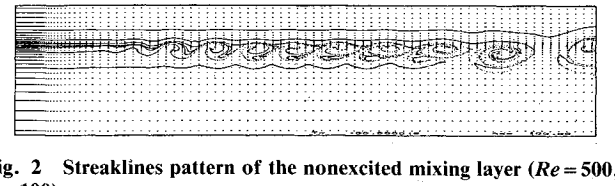

**Fig. 2 Streaklines pattern of the nonexcited mixing layer ($Re = 500$, $T = 100$).**

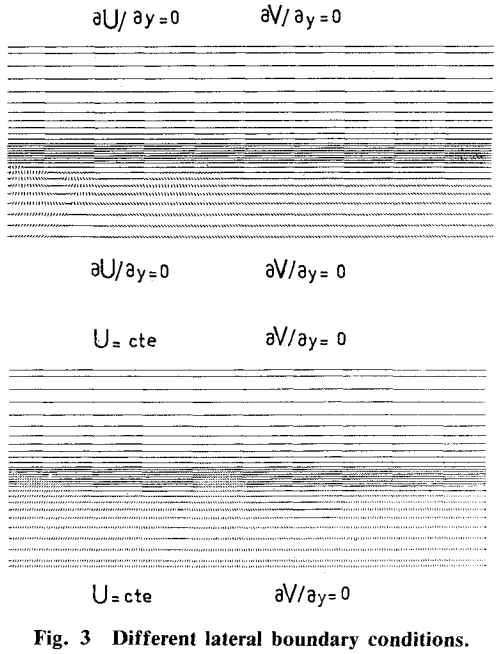


**Fig. 3 Different lateral boundary conditions.**

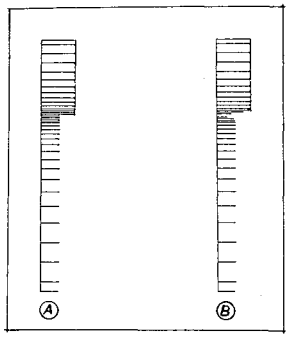


Fig. 4 Inlet boundary conditions.

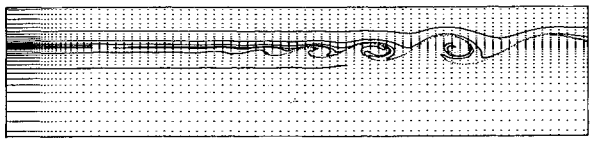

Fig. 5 Evolution of streaklines in the mixing layer, case A ($Re=200$, $T=80$).

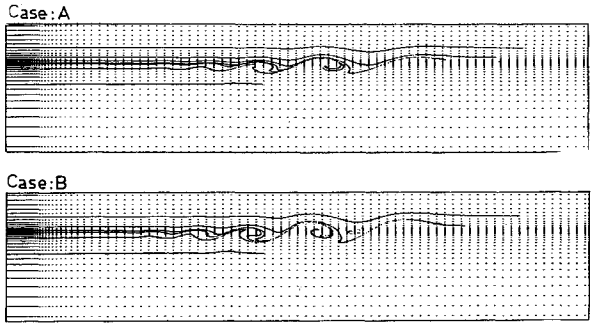


Fig. 6 Comparison between both cases.

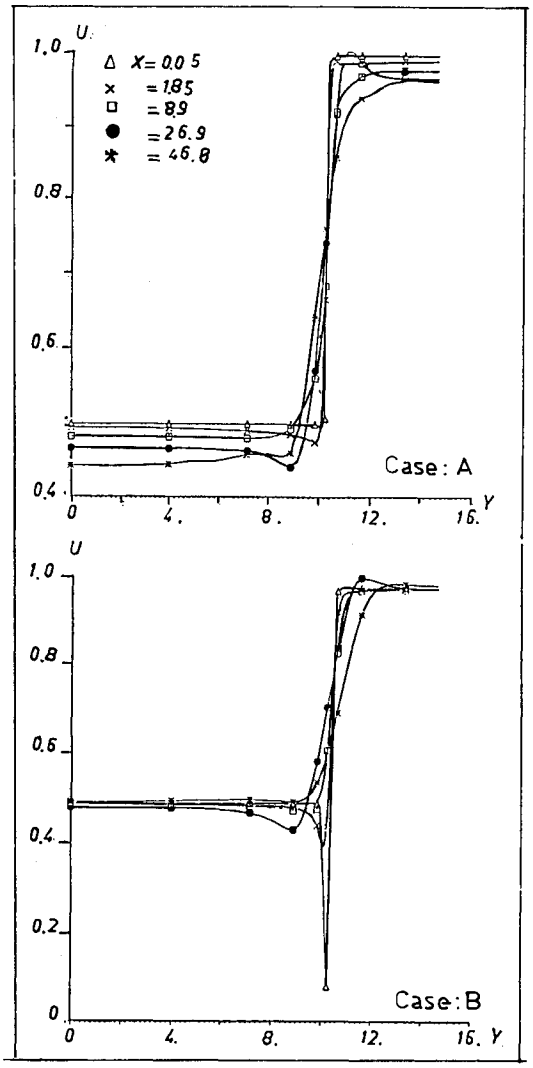


Fig. 7 $U$ velocity profiles at different sectons for the cases A and B ($Re=200$).

case A. Case B concerns the mixing layer formed by the merging of two streams initially spearated by a thin surface. This configuration represents the flow developing past the trailing edge of a thin flat plate. In order to simulate more accurately the development of the boundary layer on the flat plate, the analytic Blasius $U$ velocity profile is used for the inlet boundary, with the $V$ component set equal to zero. Theoretically, the inlet $V$ component in this case does not vanish, but is very small relative to the $U$ component. Furthermore, at the adjacent vertical section to the inlet boundary, the $V$ component is no longer zero in the present calculation, but is generated by the solution of the Navier-Stokes equations. For these reasons, the fact of setting $V=0$ at the inlet boundary does not affect the results very much.

The results are discussed here in three parts, according to physical phenomena of interest in analysing the mixing layer: analysis of the flow regions, expansion laws, and analysis of the instabilities of the mixing layer structures. The Reynolds numbers investigated are 200, 500, and 1000.

Section III B discusses the forced mixing layer. The coalescence mechanism and the nonlinear interactions among different modes are then examined.

### A. Analysis of the Natural Instability (Unforced Mixing Layer)

*Different Regions of Flow*

Both cases A and B present similar evolutions, as shown in Fig. 4. The basic mechanisms governing the development of the mixing layer are pointed out with the help of streaklines. Hence, strong merging occurs in the velocity-gradient region between the two freestreams. The development of mixing layers is initially dominated by a linear instability mechanism. The streaklines, issued from the upstream section, show that the flow is steady at the beginning. All of the lines are parallel in this zone. The instability waves are detected farther downstream. This instability grows gradually downstream and leads to the roll-up process.

A striking illustration of the development of the mixing layer is provided by Fig. 5, at $T=80$ for case A. Three different zones are observed: 1) the laminar region located near the inlet section in which the evolution of the streaklines is regular and no instability appears; 2) a region in which instability waves appear and grow progressively ($20<X<37$); and 3) a region in which the eddies result from the adverse pressure gradients occurring at this region and convecting downstream regions 1 and 2 are marked by the linear instability mechanism, while the mechanism of region 3 seems to be periodic. Region 3 corresponds to the nonlinear regime characterized by the roll-up process as pointed out by Freymuth.[7]

The difference between cases A and B is that in case B the instability appears earlier than in the other case, but the mechanisms are basically the same in both cases (Fig. 6).

*Velocity Profiles and Expansion Rates*

The velocity distribution across the mixing layer are given in Fig. 7 for the $U$ component of case A at different sections. They show a variation similar to the one reported by Bouriot.[6] This distribution is in agreement with the

spreading rates of the mixing layer. Indeed, the velocity gradient decreases with downstream distances.

The thickness of the mixing layer is defined as the transverse distance between the streamlines corresponding to $U=0.95\times U_1$ and $U=1.05\times U_2$. The results are plotted in Fig. 8 and show that the spreading of mixing layer agrees with the analytical law as established by Liepmann and Laufer[18] in the laminar case. Indeed, in the first region ($X<20$), the spreading can be written as follows:

$$b=k\cdot X^{1/2}$$

It can be seen also that the spreading rate seems to be linear up to $X=20$ for $Re=200$. Therefore, the mixing layer is laminar in the first region, whereas the expansion law is like the one of laminar-to-turbulent transition beyond this zone.

This aspect is in agreement with the experimental results of Ho and Huang.[10] It also agrees with the computational results of McInville et al.[19] in the laminar region. In the latter study, the linear growth rate in the unforced case is not detected because no vortex formulation was observed.

In case B, the behavior seems to be identical, except for the region near the inlet section (Fig. 7). In fact, in the first sections, a wake effect is detected in the $U$ velocity profiles. This wake effect explains the fact that the instability appears earlier in this configuration. Indeed, the deceleration created by the wake effect strengthens the velocity gradient and this leads to a more pronounced instability.

The results of the $V$ velocity component are given in Fig. 9, in order to complete the previous analysis. The agreement with the $U$ component seems to be good. In fact, at $T=100$ and for the sections represented on Figs. 7 and 9, the space variation of components $U$ and $V$ are due to the development of the eddies and their position relative to the section chosen. Hence, in the low-speed side, $\partial U/\partial X$ is negative, whereas $\partial V/\partial Y$ is found to be positive. This behavior could be inversed if other sections were chosen.

In the high-speed side, the change in sign obtained for $(\partial U/\partial X)$ is due to the convection of the vortices in that region.

In any case, whenever $\partial U/\partial X$ is negative, $\partial V/\partial Y$ is positive and vice versa. Hence, the continuity equation is verified at any point. This is also checked by the values of div($V$), which are found to be less than $10^{-5}$ in the whole field, as it is also discussed in Section II.B.

Moreover, the distribution of the $V$ component allows delimiting of the vortex region (Fig. 9). In fact, this component changes its sign on both sides of a vortex structure for the whole lateral section. This change of sign occurs progressively through each vertical section.

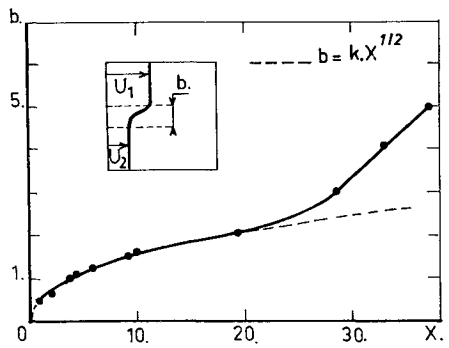


**Fig. 8 Spreading rate of the nonexcited mixing layer.**

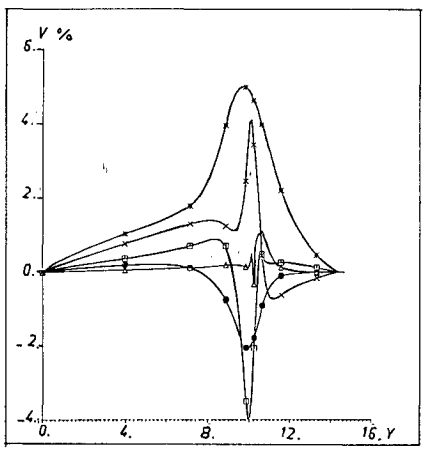


**Fig. 9 $V$ velocity profiles at different sections, case A ($Re=200$).**

### B. Analysis of Instability of Mixing-Layer Structures

*Time-Dependent Velocity and Pressure*

The time-dependent velocity components and pressure are shown in Fig. 10. It can be seen that their oscillations are periodic. The frequency of these oscillations agrees with that observed in the streakline plots. Near the inlet section the in-

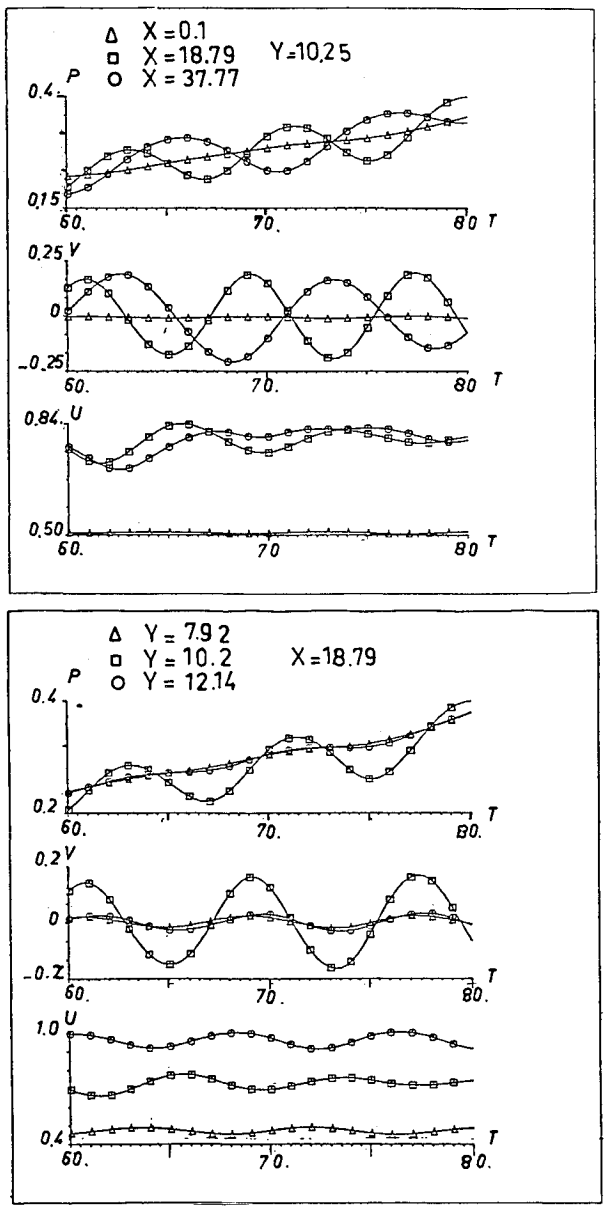


**Fig. 10 Traces of velocity and pressure in the mixing layer.**

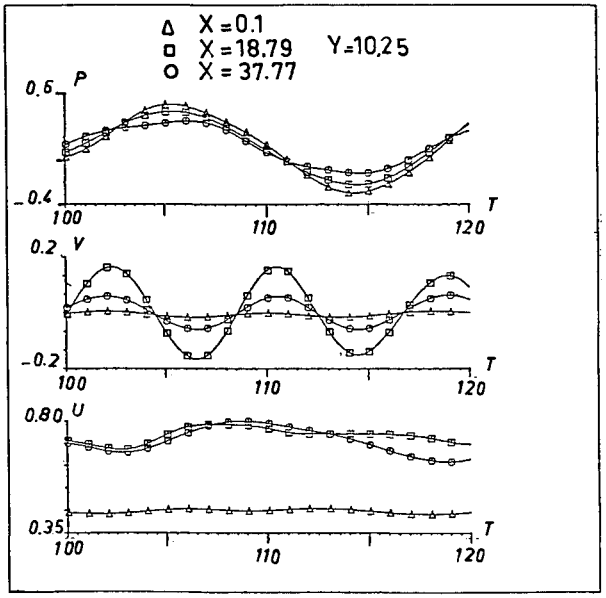


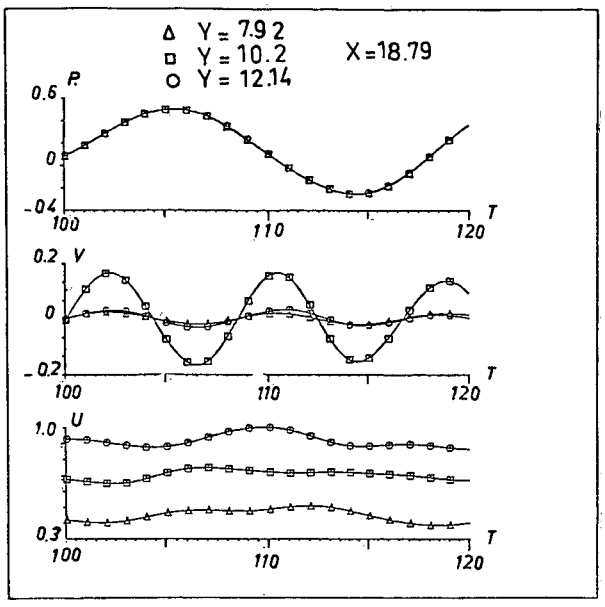


Fig. 11 Traces of velocity and pressure $100 < T < 120$.

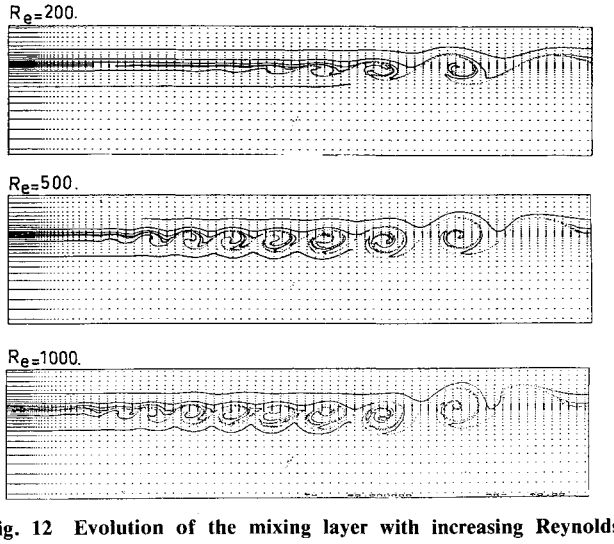


Fig. 12 Evolution of the mixing layer with increasing Reynolds number.

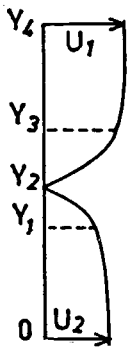


Fig. 13 Definitions of quantities in Eqs. (11).

tensity of oscillations is weak, but it grows downstream. It becomes higher in the transition zone.

The oscillations of the velocity components and pressure are strong in the mixing layer (Fig. 10). On both sides of mixing layer, weaker induced oscillations are detected.

Oscillations obtained in the time interval (100–120) for Reynolds number $Re = 500$ allow us to detect a subharmonic component $f_n/2$. In fact, the pressure oscillations show generation of this subharmonic (Fig. 11). Experimental results of Sato[20] and Freymuth[7] have pointed out that the emergence of a subharmonic component at half-frequency of the fundamental constitutes one of the most striking features in the mixing-layer dynamics. The selective growth of the subharmonic component leads farther downstream to the pairing of neighboring vortices.[11] The successive mergings of vortices is reported in these studies as the primary process governing the streamwise growth of the mixing layer. In this case, the pairing mechanism is not observed in the unforced mixing layer. In Sec. II. B, forcing is applied at the subharmonic component $f_n/2$ to obtain the coalescence mechanism.

*Reynolds Number Effects*

The viscous effect plays an important role in both determining the laminar or turbulent state of the initial free shear layer and the transition in the mixing layer. Indeed, the downstream development of shear layers is known to be very sensitive to the laminar or turbulent state. The streamwise variation of mixing-layer thickness may be parabolic or linear depending upon to laminar or turbulent state, respectively.

The viscous effect is studied by maintaining constant the velocity ratio $r = (U_1 - U_2)/(U_1 + U_2)$ and by varying the Reynolds number $Re = U_{\text{ref}} \cdot L_{\text{ref}}/\nu$. Three values of Reynolds number (200, 500, 1000) are selected.

It is found that the intitial layer grows as $X^{1/2}$, like the laminar mixing layer, for the three cases (Fig. 12). Owing to the unsteady development, the mixing layer grows linearly farther downstream, in accordance with the law predicted by the turbulent steady-state theory. This behavior is due to the stronger diffusion characterized by the rolling-up process. Three characteristic zones of the evolution of mixing layer can be detected, and the lengths of which decrease with the Reynolds number. This can be observed in the streakline plots of Fig. 12. In fact, the onset of waves moves upstream with increasing Reynolds number. The natural frequency of the mixing layer increases with Reynolds number.

The position $X_1$, where the instability waves start, as well as the distance $X_2$, where the roll-up process takes place are given in Table 2. It can be seen that those positions move upstream when the Reynolds number increases. The values of frequency of the instability waves are also given in Table 2.

This analysis agrees with Freymuth's[7] classification, which distinguishes linear and nonlinear transition regimes. The roll-up process appears in the nonlinear region. The present numerical visualization shows the laminar and transition regimes. In the linear zone, the instability waves occur, grow, and lead far downstream to the nonlinear zone where the roll-up process takes place.

**Table 2 Reynolds number effects**

| *Re* | $X_1$ | $X_2$ | *l* | *F* |
|---|---|---|---|---|
| 200 | 20.3 | 37.2 | 8 | 0.092 |
| 500 | 10.8 | 21.43 | 5.64 | 0.13 |
| 1000 | 6.7 | 17 | 5 | 0.15 |

### C. Analysis of Vortex Interaction Mechanism in the Forced Mixing Layer

In this section, a forcing technique is applied to analyze the coalescence mechanism and nonlinear interaction. The mixing layer is then excited either at $f_n/2$ (the first subharmonic) or at $f_n/a$ ($a$ being a noninteger, here $a=6.94$), respectively. The forcing is applied in the inlet section by varying the direction of the velocity $V$ at the inflexion point. In this case, the initial condition are

$$U(X_m,Y)=U_2=0.5,\quad V(X_m,Y)=0,\quad 0<Y<Y_1$$

$$U(X_m,Y)=U_2\cdot\cos\{A\cdot\sin[2\cdot\pi\cdot f_f\cdot(t-t_0)]\},\quad Y_1<Y<Y_2$$

$$V(X_m,Y)=U_2\cdot\sin\{A\cdot\sin[2\cdot\pi\cdot f_f\cdot(t-t_0)]\}$$

$$U(X_m,Y)=U_1\cdot\cos\{A\cdot\sin[2\cdot\pi\cdot f_f\cdot(t-t_0)]\},\quad Y_2<Y<Y_3$$

$$V(X_m,Y)=U_1\cdot\sin\{A\cdot\sin[2\cdot\pi\cdot f_f\cdot(t-t_0)]\}$$

$$U(X_m,Y)=U_1=1,\quad V(X_m,Y)=0,\quad Y_3<Y<Y_4 \qquad (12)$$

where $t_0$ is the time value for the fully developed mixing layer and $Y$ and $U$ as shown in Fig. 13.

This kind of forcing can qualitatively simulate the oscillations induced by the trailing edge of an airfoil or the periodic motion of the separation points of the flow past a circular cylinder. In this case, the Reynolds number is 500.

*Excitation at First Subharmonic*

In the first case ($f_f=f_n/2$), the choice of this frequency is governed by the fact that the selective growth of the subharmonic component leads downstream to the pairing of vortices, as was observed experimentally by Freymuth.[7] The sequential mergings are responsible for most of the entrainment into the shear layer and the occurrence of small-scale transition.[2,11]

When forcing is applied, the neighboring vortices are laterally displaced, having different convective velocities. Hence, they wrap around each other to form a single structure (Fig. 14). The pairing of vortices is directly related to the development of the subharmonic, as pointed out by Ho and Huerre.[11] Indeed, the wave at frequency ($f_f=f_n/2$) amplifies and the vortices are displaced until they become adjacent. The roll-up process is completed at the section where the response frequency $f_r$ reaches its maximum value. The shear-layer spreading rate is, therefore, increased by the occurrence of the pairing. This interaction is observed in a transient phase, after which the forcing frequency controls the shedding of vortices. These are emitted at a frequency of $f_n/2$.

The same behavior can be seen in the experimental study of Ho and Huang[10] and in the numerical results of McInville et al.[19] in mode II.[21]

The time-dependent velocity components and pressure are shown in Fig. 14 along the horizontal line $Y=10.25$, being near the vortex centers. The $U$ and $V$ component oscillate with the forcing frequency near the inlet section at $X=0.1$. The $V$ component plots show the existence of the natural frequency superimposed on the forcing one. At the same points, the $U$ component does not oscillate regularly, owing to the variation of the convective velocity of the eddies. This

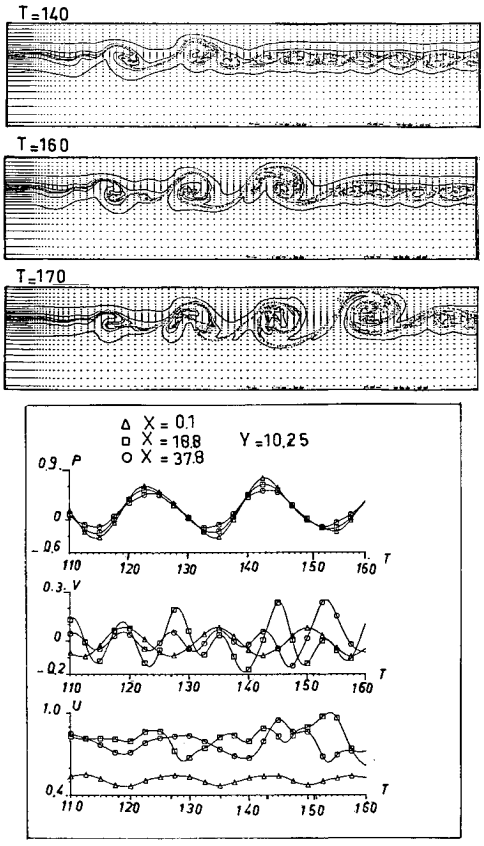


**Fig. 14 Numerical simulation of the excited shear layer ($Re=500$, $f_f=f_n/2$).**

behavior is necessary to obtain pairing phenomena. The variation of the convective velocity is due to the forcing. The pressure oscillations are in phase in all sections. Hence, forcing perturbation propagates in the flow domain through the pressure field in the same manner as acoustic waves. The pressure oscillates with a frequency near the first subharmonic in the whole field.

*Excitation at an Incommensurate Frequency*

In the second case, forcing at a frequency $f_f=f_n/a$, with a noninteger value for $a$, is applied. This excitation is imposed to study the nonlinear interaction between two different frequencies, as it is observed in the flow past a circular cylinder.[22]

The effect of this forcing is shown in Fig. 15. Pairing is also observed; but, in contrast with the previous case, this mechanism is irregular. Single vortices at the natural frequency can be found among those forming pairs. The time-dependent evolution of the velocity and pressure probably contain a complex set of interaction frequencies, as is observed in the formation zone of the wake vortices behind the circular cylinder.[23]

The time-dependent velocity components and pressure show a nonlinear interaction between the natural and forced frequencies. In fact, the pressure oscillations indicate the generation of a $(f_n/2-f_f)$ frequency resulting from the interactions (Fig. 15). It agrees with the results of Miksad et al.[24] These pressure oscillations are also found to be in phase in the whole domain. The $V$ component oscillates at $(f_n-f_f)$ and shows the interaction between the forcing and natural frequencies, as can be observed at the points $X=18.77$ and 37.77. $U$ component oscillations are more irregular than in the first case and show a nonlinear interaction between two different frequencies related to the irregular pairing mechanism. This irregularity affects the $U$ component rather than the $V$ one.

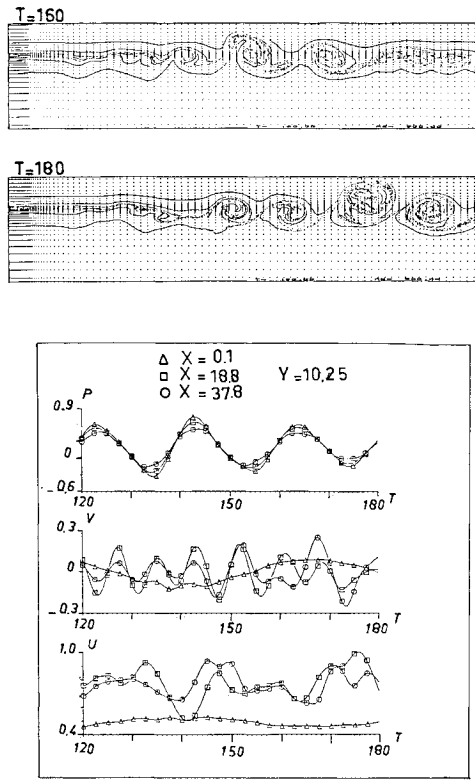


**Fig. 15 Numerical simulation of the excited shear layer ($Re=500$, $f_f=f_n/a$, $a=6.94$).**

## IV. Conclusion

Physical aspects of a plane mixing layer are analyzed by numerically solving the time-dependent Navier-Stokes equations, using a pressure velocity formulation.

In the first cases, with no forcing applied, the numerical solution reveals successively a laminar zone and linear and nonlinear transition zones. In the nonlinear zone, a roll-up process occurs and the shedding is periodic. The large-scale structures are naturally generated without imposing any perturbation. They are an intrinsic property of the Navier-Stokes equations. The spreading of mixing layer agrees with the analytical law in the steady region. In the unsteady region, this spreading is similar to the classical analytical law of turbulent steady flow. This feature is a result of roll-up process. The beginning of the transition zone moves upstream and the natural frequency increases as the Reynolds number increases.

In the second case, a forcing at the first subharmonic frequency is applied in order to analyze the coalescence mechanism. Pairing is then observed leading to the growth of the spreading rate of the mixing layer. After a transient time, the forcing frequency governs the shedding of vortices.

To examine the nonlinear interaction between two different frequencies, forcing is applied at an incommensurate frequency. The coalescence mechanism is again observed, but its structures are irregular. This phenomenon is characterized by the appearance of interaction frequencies $(f_n-f_f)$ and $(f_n/2-f_f)$.

## References

[1]Brown, G. L. and Roshko, A., "On Density Effects and Large Structure in Turbulent Mixing Layer," *Journal of Fluid Mechanics*, Vol. 83, Pt. 4, 1974, pp. 641-671.

[2]Winant, C. D. and Browand, F. K., "Vortex Pairing: The Mechanism of Turbulent Mixing Layer Growth at Moderate Reynolds Number," *Journal of Fluid Mechanics*, Vol. 41, No. 6, 1974, pp. 388-396.

[3]Michalke, A., "The Instability of Free Shear Layers," *Progress Aerospace Sciences*, Vol. 12, 1972, pp. 213-239.

[4]Huerre, P., "Nonlinear Instability of Free Shear Layers," *Laminar-Turbulent Transition*, AGARD CP 224, 1977, pp. 5-1—12.

[5]Aref, H., "Integrable, Chaotic and Turbulent Vortex Motion in Two-Dimensional Flows." *Annual Review of Fluid Mechanics*, No. 15, 1983, pp. 345-389.

[6]Bouriot, M., "Contribution a l'Etude de la Simulation Numérique de la turbulence," Thése de Docteur Es-sciences, Université de Poitiers, Poitiers, France, 1984.

[7]Freymuth, P., "On Transition in Separated Laminar Boundary Layer," *Journal of Fluid Mechanics*, Vol. 25, No. 6, 1966, pp. 683-704.

[8]Monkewitz, P. A. and Huerre, P., "Influence of the Velocity Ratio on the Spatial Instability of Mixing Layers," *The Physics of Fluids*, Vol. 25, No. 7, 1982, pp. 1137-1143.

[9]Browand, F. K. and Latigo, B. O., "Growth of the Two Dimensional Mixing Layer from a Turbulent and Nonturbulent Boundary Layer," *The Physics of Fluids*, Vol. 22, No. 6, 1979, pp. 1011-1019.

[10]Ho, C. M. and Huang, L. S., "Subharmonics and Vortex Merging in Mixing Layers," *Journal of Fluid Mechanics*, No. 16, 1982, pp. 443-473.

[11]Ho, C. M. and Huerre, P., "Perturbed Free Shear Layers," *Annual Review of Fluid Mechanics*, No. 16, 1984, pp. 365-424.

[12]Braza, M., "Simulation numérique du décollement instationnaire externe par une formulation vitesse-pression. Application a l'écoulement autour d'un cylindre," Thése de Docteur Ingénieur, Université de Toulouse, Toulouse, France, 1981.

[13]Chorin, A. J., "A Numerical Method for Solving Incompressible Viscous Flow Problems," *Journal of Computational Physics*, Vol. 2, 1967, pp. 12-26.

[14]Peaceman, D. W. and Rachford, H. H., "The Numerical Solution of Parabolic and Elliptic Differential Equations," *Journal of the Society of Industrial and Applied Mathematics*, Vol. 3, No. 1, 1955, pp. 28-41.

[15]Batchelor, B. K. (ed.), *The Collected Works of G. I. Taylor*, Vol. 2, Cambridge University Press, London, 1960.

[16]Braza, M., Haminh, H., and Chassaing, P., "Numerical Simulation of the Vortex Shedding Past a Circular Cylinder Using a Pressure-Velocity Formulation," *Numerical Methods for Transient and Coupled Problems*, edited by R. W. Lewis, E. Hinton, P. Betess, and B. A. Schrefler, Pineridge Press, 1984.

[17]Braza, M., Chassaing, P., and Haminh, H., "Numerical Study and Physical Analysis of the Pressure and Velocity Fields in the Near Wake of a Circular Cylinder," *Journal of Fluid Mechanics*, Vol. 165, 1986, pp. 79-130.

[18]Liepmann, H. W. and Laufer, J., "Investigation of Free Turbulent Mixing," NACA TN 1257, 1947.

[19]McInville, R. M., Gatski, T. B., and Hassan, H. A., "Analysis of Large Vortical Structures in Shear Layers," *AIAA Journal*, Vol. 23, Aug. 1985, pp. 1165-1171.

[20]Sato, H., "Further Investigation on the Transition of Two-Dimensional Separated Layer at Subsonic Speed," *Journal of the Physical Society of Japan*, Vol. 14, 1959, pp. 1797-1810.

[21]Davis, R. W. and Moore, E. F., "A Numerical Study of Vortex Merging in Mixing Layers," *The Physics of Fluids*, Vol. 26, June 1985, pp. 1626-1635.

[22]Kourta, A., "Analyse physique et simulation numérique des structures tourbillonnaires du sillage proche d'un cylindre circularie," Thése de Docteur Ingénieur, Université Toulouse, Toulouse, France, 1984.

[23]Kourta, A., Boisson, H. C., Braza, M., Chassaing, P., and Haminh, H., "Wake-Shear Layer Interaction and the Onset of Turbulence Behind a Circular Cylinder," Paper presented at Fifth Symposium on Turbulent Shear Flows, New York, Aug. 1985.

[24]Miksad, R. W., Jones, F. L., Powers, E. J., Kim, Y. C., and Khadra, L., "Experiments on the Role of Amplitude and Phase Modulation during Transition to Turbulence," *Journal of Fluid Mechanics*, Vol. 123, 1982, pp. 1-29.